Title

Coupled nonhomogeneous flows and flow-enhanced concentration fluctuations during startup shear of entangled polymer solutions

Journal

Physical Review Fluids, 5(4)

ISSN

2469-9918

Authors

Burroughs, Michael C
Shetty, Abhishek M
Leal, L Gary
et al.

Publication Date

2020-04-01

DOI

10.1103/physrevfluids.5.043301

Peer reviewed

Supporting information for

“Coupled non-homogeneous flows and flow-enhanced concentration fluctuations during startup shear of entangled polymer solutions”

Michael C. Burroughs,[1] Abhishek M. Shetty,[2] L. Gary Leal[1], and Matthew E. Helgeson[1]

1. Department of Chemical Engineering, University of California, Santa Barbara, Santa Barbara, California 93106 United States
2. Anton Paar USA Inc., Ashland, Virginia 23005 United States

Homogeneous Rolie-Poly model formulation

The Rolie-Poly [1] constitutive model is a simplified, single-mode form of the detailed GLaMM [2] model for entangled polymers. Predictions of the Rolie-Poly model agree well with both linear and nonlinear rheological data [1]. In the Rolie-Poly model, the time derivative of the polymer conformation tensor is given by

$$\frac{\partial}{\partial t}Q_{r\theta}=\frac{-Q_{r\theta}}{\tau_d}-\frac{2}{\tau_R}\left(1-\sqrt{\frac{3}{tr(Q)}}\right)\left(Q_{r\theta}+\left(\frac{tr(Q)}{3}\right)^{\frac{-1}{2}}Q_{r\theta}\right)+\dot{r}\frac{\partial}{\partial \dot{r}}\left(\frac{u}{\dot{r}}\right)Q_{rr} \tag{1}$$

$$\frac{\partial}{\partial t}Q_{rr}=\frac{1-Q_{rr}}{\tau_d}-\frac{2}{\tau_R}\left(1-\sqrt{\frac{3}{tr(Q)}}\right)\left(Q_{rr}+\left(\frac{tr(Q)}{3}\right)^{\frac{-1}{2}}\left(Q_{rr}-1\right)\right)+2\dot{r}\frac{\partial}{\partial \dot{r}}\left(\frac{u}{\dot{r}}\right)Q_{r\theta} \tag{2}$$

$$\frac{\partial}{\partial t}Q_{\theta\theta}=\frac{1-Q_{\theta\theta}}{\tau_d}-\frac{2}{\tau_R}\left(1-\sqrt{\frac{3}{tr(Q)}}\right)\left(Q_{\theta\theta}+\left(\frac{tr(Q)}{3}\right)^{\frac{-1}{2}}\left(Q_{\theta\theta}-1\right)\right) \tag{3}$$

where Q is the stress tensor with subscripts indicating the various components, u is the flow direction of the velocity vector, τ_d is the time for relaxation by reptation, τ_R is the Rouse relaxation time relevant to chain stretch. To solve for the transient stresses and obtain the velocity profile, the Rolie-Poly constitutive equation was coupled with the equations of motion in cylindrical coordinates for the creeping flow limit ($\Re=0$). For a 1D flow

$$\frac{\partial}{\partial \theta}u=0 \tag{4}$$

$$\frac{1}{\acute{r}^2}\frac{\partial}{\partial \acute{r}}\left[\acute{r}^2\left(\varpi \acute{r}\frac{\partial}{\partial \acute{r}}\left[\frac{u}{\acute{r}}\right]+\sigma_{r\theta}\right)\right]=0 \quad (5)$$

where ϖ is the ratio of the solvent viscosity to polymer viscosity, u is the fluid velocity in the flow direction, and $\sigma_{r\theta}$ is the shear stress. The stress is computed from the polymer conformation tensor

$$\sigma=G(Q-I) \quad (6)$$

where G is the shear modulus. The constitutive equation and equations of motion were solved numerically using the ode15s integration scheme in MATLAB. The Rolie-Poly model predictions of the constitutive curve were calculated by solving the constitutive equations for steady state assuming a constant velocity gradient over a range of Wi, where

$$Wi=\tau_d\dot{\gamma} \quad (7)$$

and $\dot{\gamma}$ is the applied shear rate.

Complications of nonlinear rheology measurements in entangled polymer solutions

The non-homogeneous velocity profiles just described during the startup of steady shear in highly entangled PS/DOP are reminiscent of similar profiles observed in other highly entangled polymer solutions [3]. In such cases, there has been some debate in the literature as to the possibility that such non-homogeneous flows could arise due to the influence of boundary effects [4–7] or other artifacts associated with the flow protocol [8]. Specifically, we acknowledge several phenomena that could possibly contribute to the transient, inversely-bowed velocity profiles we observed at higher levels of entanglement in PS/DOP: edge fracture, wall slip, and the Deborah number of startup shear. In the following discussion, we explore whether any of these phenomena affect the observed inversely-bowed velocity profiles.

Edge fracture occurs in entangled polymer rheology due to large values of the second normal stress difference, N_2. Specifically, the onset of edge fracture was found to obey the criterion

$$\frac{1}{2}\Delta\sigma\frac{d\left|N_2(\dot{\gamma})\right|}{d\dot{\gamma}}>\frac{2\pi\Gamma}{L_y} \quad (8)$$

where $\Delta\sigma$ is the shear stress difference across the free surface (i.e. fluid and air), Γ is the surface tension of the free surface, and L_y is the geometry gap thickness [9]. When present, edge fracture can result in macroscopic perturbations to the air-liquid interface and, in turn, it is believed to impact the internal flow field during the viscometric measurement [4,5,9–12]. In cone-and-plate geometries, it is difficult to observe the propagation of edge fracture and how it impacts the internal flow field. Recently, it was argued that the presence of edge fracture could be the source of measured non-homogeneous velocity profiles [4]. However, experiments have shown that edge fracture acts to homogenize the flow field [13]. Some researchers have attempted to circumvent edge fracture by employing a partitioned cone and plate system. Others have used a Taylor-Couette flow cell identical to the one used in this study, and monitored the height of the meniscus as edge fracture develops [10].

In the measurements presented here, a custom-fabricated stainless-steel lid was utilized to delay the occurrence of edge fracture to high *Wi* by effectively eliminating the free surface (i.e. air-fluid interface). As shown in Figure 1, edge fracture is minimized when the stainless-steel lid is placed on top of the sample. The use of a lid to minimize the free surface in Taylor-Couette flow is found to extend the possible applied shear rate where perturbations of the top surface are observed by over an order of magnitude. All measurements were performed well below this determined maximum applied shear rate.

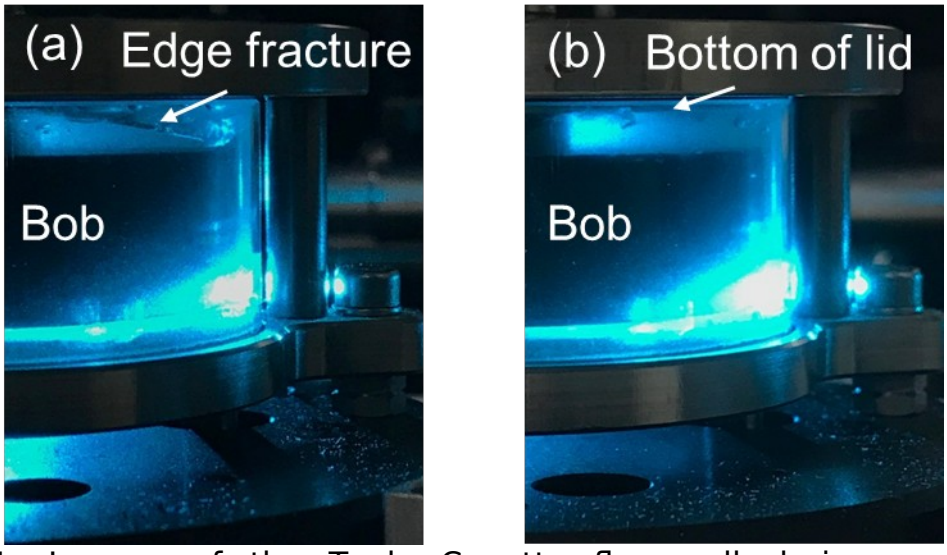

Figure 1. Images of the Taylor-Couette flow cell during a rheo-PTV experiment of 10 wt % PS(8.42M)/DOP at Wi=5.5 (a) without and (b) with a stainless-steel lid on top of the fluid.

Wall slip in entangled polymer solutions has been investigated thoroughly [14–16]. In particular, entangled polystyrene solutions are known

to slip under shear flow on a quartz surface, where the magnitude of the slip velocity depends on the shear stress at the interface (in this case, the outer stationary wall). Based on the mechanism of polymer slip proposed by de Gennes, the thickness of fluid comprising a slip boundary layer should be restricted to a length scale on the order of the polymer's radius of gyration [17,18]. Such nanometer length scales are unobservable in rheo-PTV measurements, therefore wall slip reduces the measured bulk shear rate due to the non-zero velocity at the stationary wall. This is consistent with what is observed in the steady state velocity profiles for the fluids with Z = 30 and Z = 36 samples, but transiently we observe a region of higher shear rate than the bulk adjacent to the stationary wall.

To quantify the presence of wall slip, the measured velocity profile near the stationary wall was extrapolated to determine the velocity at the wall, which yields the slip velocity (V_S). The slip velocity is found to follow two scaling regimes with measured inner wall shear stress (Figure 2(a)). At low shear stresses, the slip velocity varies with shear stress as $V_s \propto \sigma_{r\theta}^{1.4}$, corresponding to a nearly linear regime. For shear stresses in the nonlinear flow regime, the slip velocity scales as $V_s \propto \sigma_{r\theta}^{3.2}$. These scalings are consistent with previously reported slip velocity dependencies on shear stress for similar fluids [14]. Interestingly, we only observe slip at the quartz stationary wall. For flow devices in which the boundaries are composed of identical materials, we would expect wall slip to occur at both surfaces, with a higher slip velocity occurring at the moving boundary since the shear stress is highest. Although the shear stress is higher at the moving boundary, the difference in slip boundary conditions between the moving and stationary boundaries is believed to result from the different chemical composition of each surface (anodized aluminum and quartz, respectively). The determined slip velocities vary in time following the startup of shear, as expected given the shear stress dependence of slip. Figure 2(b) reveals the time dependence of slip following startup of shear at a particular Wi.The maximum slip velocity is found to occur when the inner wall shear stress overshoots shortly after the startup of flow. Following the overshoot in shear stress, the slip velocity reaches a steady value concurrent with the plateau of the shear stress.

In comparing the transient evolution of the slip velocity (Figure 2(b)) to that of the velocity profile (Error: Reference source not found(b)), it is apparent that although the wall slip and inverse-bowing appear over similar time scales concomitant with the stress overshoot, the slip velocity achieves a steady state value significantly long before the slow relaxation of the high shear region adjacent to the stationary boundary. Furthermore, at steady state wall slip is still present, whereas the flow achieves a homogeneous shear rate.

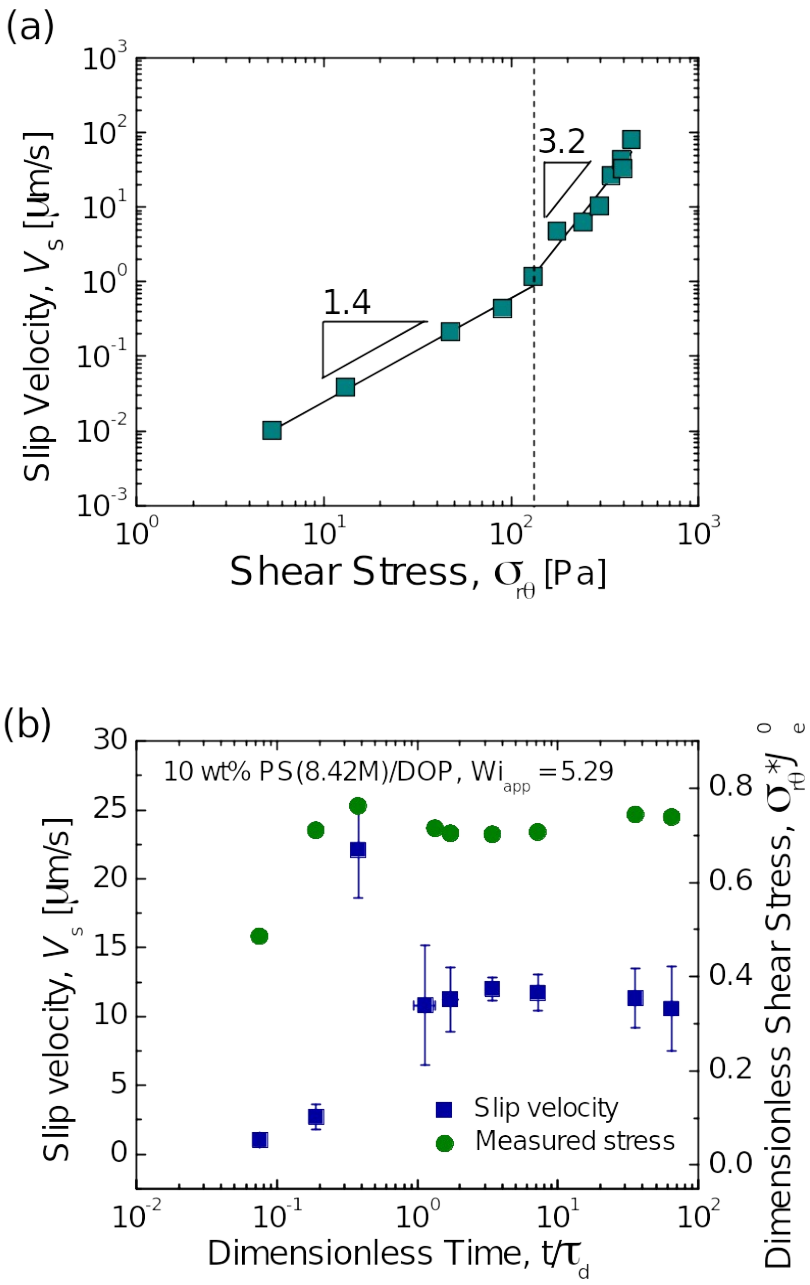

Figure 2. (a) Steady slip velocity extrapolated from rheo-PTV measurements using 10 wt% PS(8.42M)/DOP. (b) Transient slip velocities and corresponding measured shear stress.

The effect of Deborah number on the observed velocity profiles

The influence of the time for shear startup was investigated by varying the Deborah number ($De = \frac{\tau_d}{\tau_{ramp}}$), where τ_{ramp} is the time taken to reach the final velocity of the moving wall starting from rest. Figure 3(a) shows the sensitivity of the measured shear stress upon startup flow at a fixed Wi for varying De. The maximum in the shear stress decreases with decreasing De,

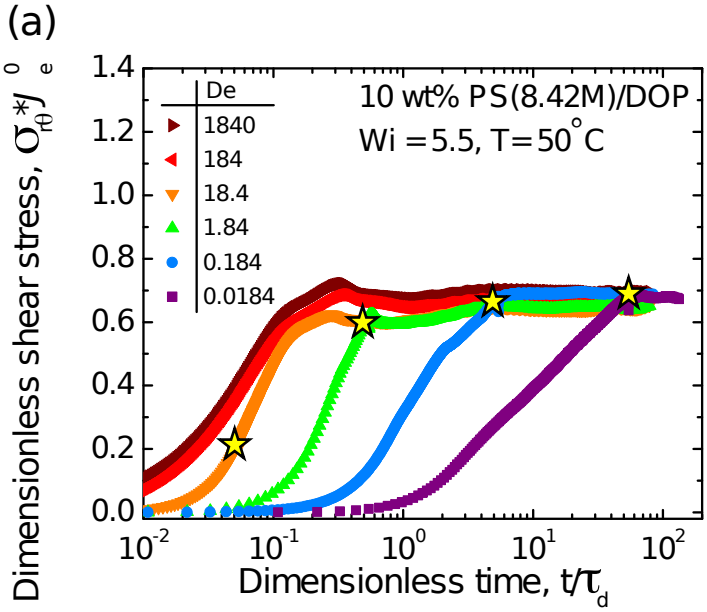

but the steady state shear stress is independent of De. The overshoot in shear stress is eliminated altogether when $De \leq 0.184$. The absence of an overshoot for $De < 1$ supports the notion that the initial overshoot in shear stress results from an over-orientation of the polymer chains. As shown in Figure 3(b), the magnitude of inverse bowing is independent of the applied value of *De*. Inverse bowing occurs for all *De* investigated, which suggests that an overshoot in the shear stress is not a necessary condition for nonhomogeneous flow in entangled polymer solutions.

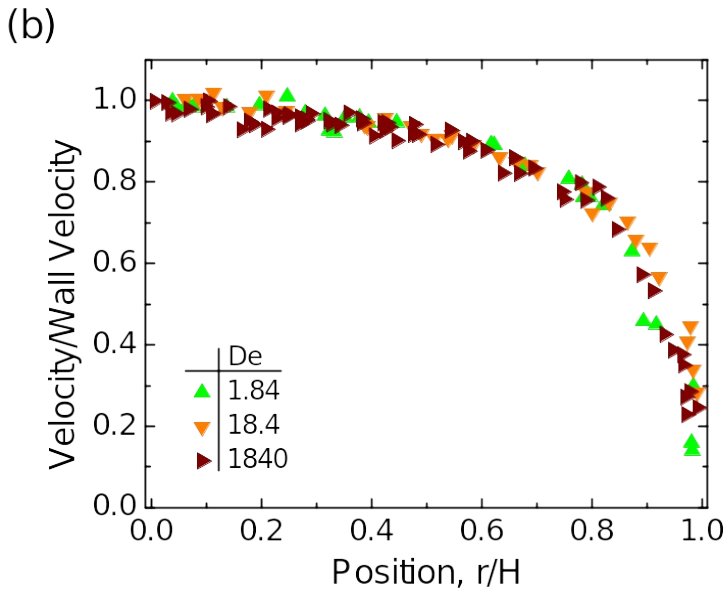

Figure 3. (a) Measured shear stress following startup shear of 10wt% PS(8.42M)/DOP at Wi=5.5 for varying De. The stars indicate the time at which the wall velocity reaches the targeted value. (b) Nonhomogeneous velocity profiles shortly after shear startup for several applied De.

At steady state, where the shear stress exhibits little change over tens of reptation times, the velocity profiles appear linear with no observable dependence on the applied *De* (Figure 4). The large standard deviation (±10%, as shown via the error bars) results from time-averaging velocimetry data over long periods of time.

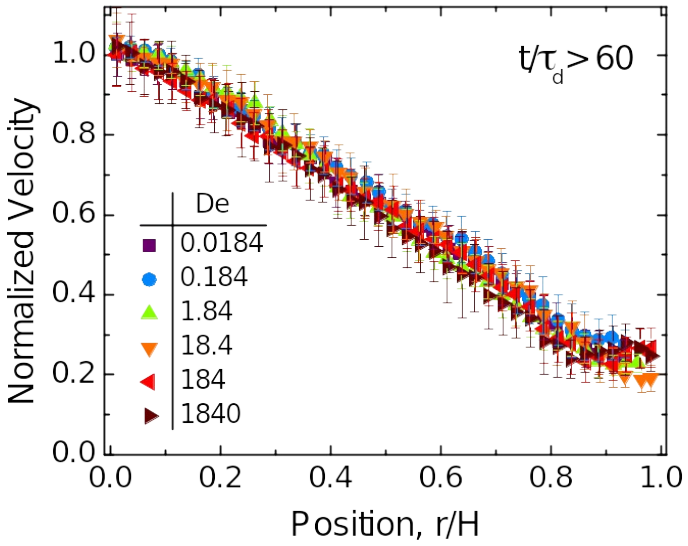

Figure 4. Steady state velocity profiles of 10 wt% PS(8.42M)/DOP for varying De and Wi=5.5.

Shear-enhanced concentration fluctuations observed in rheo-microscopy

The 1D FFT of the vertically averaged image intensity contour was calculated to provide a quantitative estimate of the characteristic length scale of shear-enhanced concentration fluctuations (Figure 5). From the peak in the 1D FFT, the characteristic length is estimated to be between 8.5 and 9.5 μm.

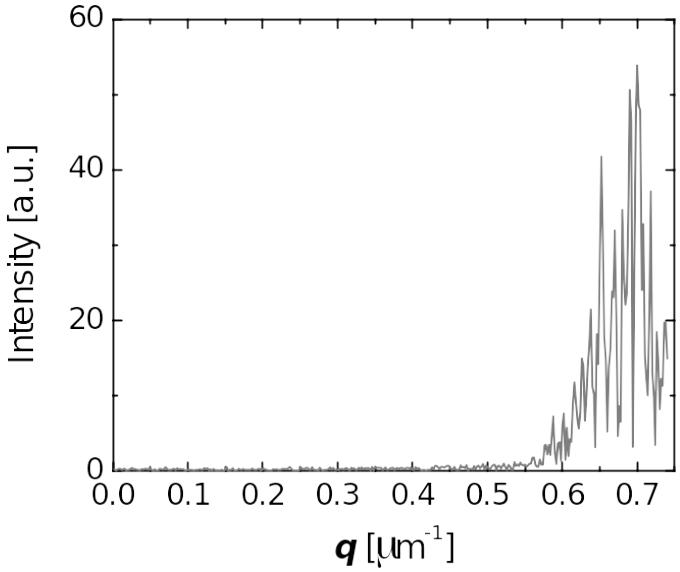

Figure 5. 1D FFT of the vertically averaged intensity contour of Figure 8 in the paper.

References

[1] A. E. Likhtman and R. S. Graham, *Simple constitutive equation for linear polymer melts derived from molecular theory: Rolie-Poly equation*, J. Nonnewton. Fluid Mech. **114**, 1 (2003).
DOI: 10.1016/S0377-0257(03)00114-9

[2] R. S. Graham, A. E. Likhtman, T. C. B. McLeish, and S. T. Milner, *Microscopic theory of linear, entangled polymer chains under rapid deformation including chain stretch and convective constraint release*, J. Rheol. **47**, 1171 (2003).
DOI: 10.1122/1.1595099

[3] Y. T. Hu, L. Wilen, A. Philips, and A. Lips, *Is the constitutive relation for entangled polymers monotonic?*, J. Rheol. **51**, 275 (2007).
DOI: 10.1122/1.2433701

[4] Y. Li, M. Hu, G. B. McKenna, C. J. Dimitriou, G. H. McKinley, R. M. Mick, D. C. Venerus, and L. A. Archer, *Flow field visualization of entangled polybutadiene solutions under nonlinear viscoelastic flow conditions*, J. Rheol. **57**, 1411 (2013).
DOI: 10.1122/1.4816735

[5] Y. Li and G. B. McKenna, *Startup shear of a highly entangled polystyrene solution deep into the nonlinear viscoelastic regime*, Rheol. Acta **54**, 771 (2015).
DOI: 10.1007/s00397-015-0876-5

[6] S. Q. Wang, G. Liu, S. Cheng, P. E. Boukany, Y. Wang, X. Li, Y. Li, M. Hu, G. B. McKenna, et al., *Letter to the Editor: Sufficiently entangled polymers do show shear strain localization at high enough Weissenberg numbers"*, J. Rheol. **58**, 1059 (2014).
DOI: 10.1122/1.4884364

[7] S. Ravindranath and S.-Q. Wang, *Steady state measurements in stress plateau region of entangled polymer solutions: Controlled-rate and controlled-stress modes*, J. Rheol. **52**, 957 (2008).
DOI: 10.1122/1.2936869

[8] S. Cheng and S.-Q. Wang, *Is shear banding a metastable property of well-entangled polymer solutions?*, J. Rheol. **56**, 1413 (2012).
DOI: 10.1122/1.4740264

[9] E. J. Hemingway, H. Kusumaatmaja, and S. M. Fielding, *Edge Fracture in Complex Fluids*, 1 (2017).
DOI: 10.1103/PhysRevLett.119.028006

[10] Y. T. Hu, *Steady-state shear banding in entangled polymers?*, J. Rheol. **54**, 1307 (2010).
DOI: 10.1122/1.3494134

[11] C. Sui and G. B. McKenna, *Instability of entangled polymers in cone and plate rheometry*, Rheol. Acta **46**, 877 (2007).

DOI: 10.1007/s00397-007-0169-8
[12] Y. W. Inn, K. F. Wissbrun, and M. M. Denn, *Effect of Edge Fracture on Constant Torque Rheometry of Entangled Polymer Solutions*, Macromolecules **38**, 9385 (2005).
DOI: 10.1021/ma0510901
[13] S. Shin, K. D. Dorfman, and X. Cheng, *Effect of edge disturbance on shear banding in polymeric solutions*, J. Rheol. **62**, 1339 (2018).
DOI: 10.1122/1.5042108
[14] V. R. Mhetar and L. A. Archer, *Slip in Entangled Polymer Solutions*, Macromolecules **31**, 8617 (1998).
DOI: 10.1021/ma971339h
[15] J. Sanchez-Reyes and L. A. Archer, *Steady shear rheology of entangled polymer liquids : Implications of interfacial slip*, J. Rheol. **46**, 1239 (2002).
DOI: 10.1122/1.1498283
[16] J. Sanchez-Reyes and L. A. Archer, *Interfacial Slip Violations in Polymer Solutions : Role of Microscale Surface Roughness*, Langmuir **19**, 3304 (2003).
DOI: 10.1021/la0265326
[17] F. Brochard and P. G. de Gennes, *Shear-Dependent Slippage at a Polymer/Solid Interface*, Langmuir **8**, 3033 (1992).
DOI: 10.1021/la00048a030
[18] H. Müller-Mohnssen, D. Weiss, and A. Tippe, *Concentration dependent changes of apparent slip in polymer solution flow*, J. Rheol. **34**, 223 (1990).
DOI: 10.1122/1.550125